CHAPTER 10

Advances in Eddy-Flux Analyses, Remote Sensing, and Evidence of Climate Change

I. INTRODUCTION

Throughout the book, we emphasize the need to identify underlying biophysical principles that can be tested at fine spatial and temporal scales, and then simplified to apply across landscapes and continents. In the first six chapters, we quantify and model the ways that carbon, water, and nutrients move in, through, and out of ecosystems. In chapters seven through nine, we introduce scaling principles and give examples of their use over increasingly larger geographic units. This new chapter does not cover the full spectrum of temporal and spatial scales outlined in Figure 1.1, rather it concentrates on new technologies applied to current conditions.

Since 1998, when we completed the 2nd edition, three major advances have significantly increased the power of multi-scale forest ecosystem analysis. First, the establishment of *regional and global networks of eddy-covariance flux towers* now provides

[1] Although NEP includes additional losses of carbon from an ecosystem through leaching, we assume such losses are well within the error estimates of eddy-flux measurements.

continuous measures of carbon, water and energy fluxes from an array of forests and other types of ecosystems. This new set of data, available in comparable format from regional and global data centers, quantifies measurements that increase our confidence in predicting ecosystem responses across landscapes, and provides a basis for generalizations.

Second, *the launch of a new generation of earth observation satellites* has lead to the production of an array of standardized and near-real time delivery of a host of important land data products. These satellite-derived products have spawned a new generation of regional scale modeling of carbon and water cycles, biogeochemistry, biodiversity, and habitat-change analyses.

Third, *clear detection of the effects of global climatic change* has been observed on forested landscapes. We provide evidence that climate change has affected not only forest growth but also the frequency and extent of disturbance and expansion of forests northward. All of these responses have important societal implications for the future.

By 2005, the number of eddy-flux sites grew to exceed 200. These instrumented sites, as described in Chapter 3, offer not only a continuous record of net ecosystem exchange (NEE), or net ecosystem production (NEP),[1] but opportunities to evaluate the underlying processes that affect CO_2 and water vapor exchange, trace gas emissions, and the general health and productivity of forests. The eddy-flux sites cover a sufficient range in productivity and environments to permit testing a host of detailed process-based models. In addition, because the area of the flux measurements must be relatively large (~1 km^2), eddy-flux sites serve as calibration points for a variety of remote sensing techniques (Section III). In this section we illustrate the extent that an expanding network of flux-measurement sites has helped improve ecosystem models, and thereby our abilities to extrapolate flux estimates with increasing confidence across landscapes and continents.

II. EDDY-COVARIANCE FLUXES

A. Gross Primary Production

Gross primary production (GPP), under near equilibrium conditions, is estimated at eddy-flux sites from the sum of net carbon exchange (NEE) measured during the day plus ecosystem respiration (R_e). Respiration is measured at night when photosynthesis is nil, and then adjusted for increases in temperature during the day.

An annual summary of carbon and water balances is presented in Table 10.1 for 17 forested sites with wide ranges in climate, stand age, LAI, and disturbance. GPP is shown to increase generally from boreal (700–1000 $g\,C\,m^2\,yr^{-1}$) through temperate (1000–2200 $g\,C\,m^2\,yr^{-1}$) to tropical and semitropical forests (2700–3200 $g\,C\,m^2\,yr^{-1}$).

Seasonal patterns in GPP differ significantly depending on the type of forest and degree of disturbance. Wet tropical forests show the highest values with little seasonal variation (Fig. 10.1). Other types show seasonality that parallels trends in solar radiation, with notable reduction in GPP where forests experience drought (e.g., Mediterranean broadleaf forests).

Because GPP and transpiration are well-understood processes, they can be modeled at a 30-minute resolution (Law *et al.*, 2002; Tuzet *et al.*, 2003). Such high temporal resolu-

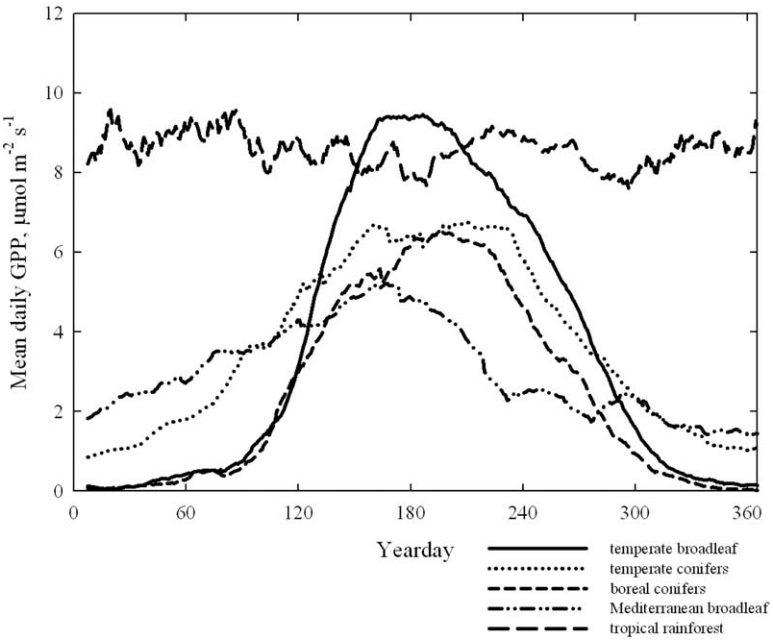

FIGURE 10.1. Seasonal patterns in gross primary production differ significantly among major forest types. Data provided courtesy of Dr. Eva Falge, Max Planck Institute, Germany. See Falge *et al*. (2002) for additional information.

tion is valuable to derive procedures to fill missing data and to account for residual errors in measurements for a wide variety of ecosystem components (Williams *et al.*, 2005). To drive models with such high temporal resolution, however, requires more precise information than is generally available across landscapes. One solution is to integrate measurements over longer time intervals (Goulden *et al.*, 1996; Law *et al.*, 2000, 2002; Turner *et al.*, 2005).

With continuous monitoring of CO_2 exchange at eddy-flux tower sites, our knowledge of the constraints on forest productivity has greatly increased. Some models focus on predicting the relative constraints on photosynthetic activity throughout the year and between years. For example, Jolly *et al.* (2005) constructed an index that identifies the extent that variation in day length, air temperature, and vapor pressure deficit limits photosynthesis. Figure 10.2 contrasts the limitations of these three variables on photosynthesis for a tropical broadleaf forest in Australia with that of cool temperate evergreen forest in Montana.

B. Ecosystem Respiration

Detailed analyses at 18 forest sites in Europe indicate that on average >70% of the respired CO_2 originates below ground (Janssens *et al.*, 2001). The efflux of CO_2 from soil represents

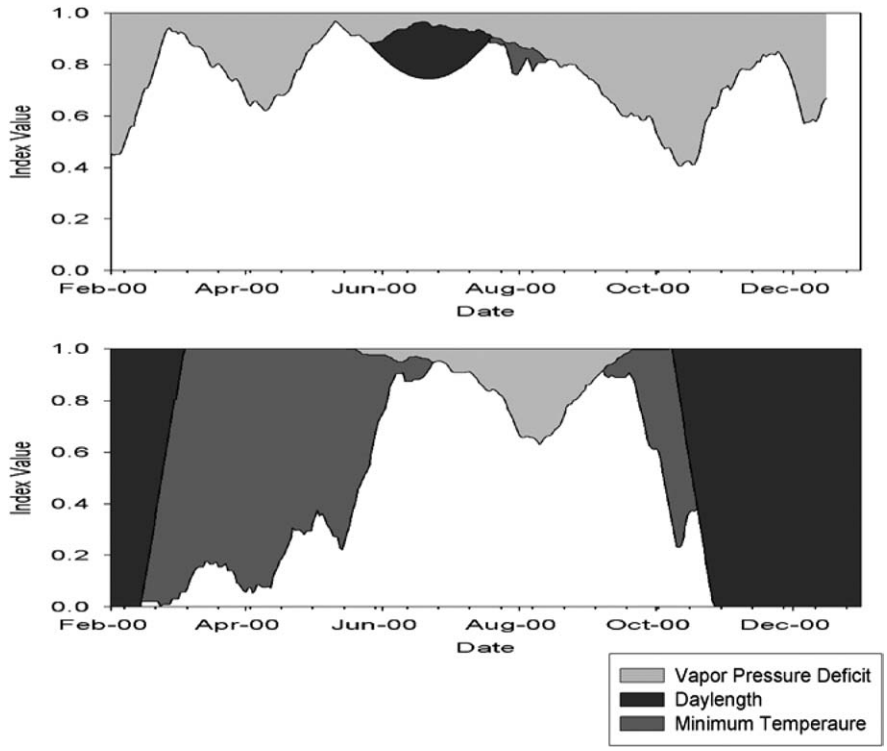

FIGURE 10.2. The relative photosynthetic activity of a tropical wet-dry rainforest in Australia (upper panel) is generally limited by high evaporative demand. Day length limits GPP for about a month and low temperatures for only a few weeks. In contrast, a temperate conifer forest in the western United States (lower panel) is limited by day length in winter, low temperatures in the spring and fall, and high evaporative demand throughout the summer. (After Jolly *et al*., 2005.)

both autotrophic (R_a) and heterotrophic (R_h) respiration. Högberg *et al.* (2001) and Bhupinderpal-Singh *et al.* (2003) discovered from tree girdling experiments that more than 50% of the soil CO_2 efflux is associated with the export of current photosynthate to roots and mycorrhizae. The fraction of GPP allocated below ground is known to decrease with increases in soil fertility (Hobbie and Colpaert, 2003; Hobbie, 2006; Johnsen *et al.*, 2007), and to result in commensurate changes in above-ground properties (e.g., increases in wood growth, foliar N content, LAI, and the ratio of actual to potential GPP).

Comparisons of R_a and R_h indicate a generally close relationship, not surprisingly, considering that litter production is associated with both NPP and GPP (Bond-Lamberty *et al.*, 2004). Although GPP can accurately be estimated at hourly and daily time steps, it remains a challenge to document what fraction of current GPP is allocated below ground at weekly and monthly intervals. Some estimate of soil fertility, directly or through its influence on canopy quantum efficiency, is essential to set limits on GPP and the fraction partitioned below ground (Chapter 3; Hobbie and Colpaert, 2003; Hobbie, 2006).

Recent models, supported from data acquired at many sites, predict soil CO_2 efflux as a function of an exponential temperature term, seasonal variation in soil water content, pore space, and maximum LAI (Reichstein *et al.,* 2003). Such models might be improved through a closer link with seasonal variation in GPP and the proportion allocated below ground (Irvine *et al.*, 2005).

C. Net Ecosystem Production (NEP)

The net amount of carbon exchanged by an ecosystem goes from positive to negative following disturbance. Undisturbed forests exhibit a ratio of NEP to GPP between ~0.1 to 0.4 (last column in Table 10.1). With disturbance, the ratio falls below zero as indicated for entries representing regenerating forests after clear-felling operations. Negative values may continue for several decades, depending on the amount of detritus present and the growth rates of planted (Gainesville, Florida) or sprouting trees (Castelporziano, Italy). Although the presence of other vegetation may contribute to a rapid increase in LAI and GPP within a few years following disturbance (e.g., Hyytiala, Finland; Bios, France), competition with tree regeneration may delay full canopy development and a return to a positive carbon balance (Gower, 2003).

Unusual climatic events, as recorded in the third year of data at Harvard Forest, can decrease the NEP/GPP ratio significantly (from >0.2 to 0.11) by increasing R_e without reducing GPP, but the ratio still remains positive. Older stands composed of a single dominant species, such as *Picea mariana* in Canada, may vacillate between being a carbon sink or source from one year to the next depending on spring and summer temperatures (Arain *et al.*, 2002). Undisturbed old-growth forests with a mixture of understory tree species, however, can be expected to maintain a positive NEP and NEP/GPP ratio (e.g., Wind River, Washington, Table 1A).

The most extreme interannual variation in NEP and NEP/GPP reported is for an old-growth *Populus tremuloides* forest in the southern boreal region of Canada, where NEP ranged from 80 to 290 $g\,C\,m^2\,yr^{-1}$ and NEP/GPP from 0.07 to 0.20 over a five-year period (Arain *et al.*, 2002). The interannual variation was attributed to spring conditions that delayed or enhanced budbreak (Arain *et al.*, 2002). On the other hand, young, fast-growing plantations, as represented by the Duke and Gaineville pine forests in Table 10.1, may produce positive ratios of NEP/GPP quickly following disturbance, particularly if soil fertility is inherently high or nutrient supplements are added (Sampson *et al.*, 2006).

D. Net Primary Production (NPP)

Net primary production (NPP) is the residual after autotrophic respiration is subtracted from GPP. To predict variation in NPP across geographic units of increasing size requires progressive simplifications in models, as emphasized in Chapter 7 and the preceding discussion. Recently, a number of simplifying features have been incorporated into predictive models of forest growth that have been widely tested on natural forests and plantations (Landsberg *et al.*, 2003). These simplifying features include expanding from daily to monthly time steps (Coops *et al.*, 2000), assuming that NPP represents an approximately constant proportion of gross photosynthesis (Fig. 3.9; Gifford, 2003; but see Cannell and Thornley, 2000), and that the fraction of NPP allocated aboveground increases with soil

TABLE 10.1

Site Characteristics of Selected Eddy-Flux Sites with Estimates of Annual Carbon and Water Balances. Negative NEP Values Represent Recently Disturbed Sites Losing Carbon to the Atmosphere

Vegetation Place name	Location Latitude & Longitude	Elev., m	Precip. (P), mm yr^{-1}	Water Balance, mm yr^{-1} P-ET	Stand age, yrs	LAI m^2m^{-2}	NEP g C m^{-2} yr^{-1}	R_e g C m^{-2} yr^{-1}	GPP[1] g C m^{-2} yr^{-1}	NEP/GPP
Evergreen conifers										
Aberfeldy, Scotland	56°N, 4°W	340	1242	355	15	8.0	487	−1270	1757	0.28
Bordeaux, France[1]	56°N, 0°E	60	995	682	30	2.8	525	−1638	2163	0.24
Duke, NC, USA	36°N, 79°W	163	748	505	17	5.2	538	−941	1479	0.36
Flakaliden, Sweden[1]	64°N, 19°E	225	520	298	31	2.0	173	−526	699	0.25
Loobos, Netherlands[1]	52°N, 6°E	25	758	419	80	3.0	323	−1114	1439	0.22
Metolius, Oregon USA[1]	44°N, 121°W	915	867	628	45/250	2.1	287	−885	1172	0.25
Wind River, Wash., USA[2]	46°N, 122°W	355	2528	NA	500	11.0	150	−1420	1570	0.13
Hyytiala, Finland[1,8]	62°N, 24°E	170	540	317	1–2	1.8	−240	−602	364	−0.66
					35	3.0	228	−720	948	0.24
Bilos, France[8]	45°N, 52°E	60	930	NA	1–2	1.9	−225	−878	602	−0.37
					54	4.0	222	−1415	1600	0.14
Gainesville, Florida, USA[3]	30°N, 82°W	46	1332	NA	1–2	0.1–3.0	−1076	−1988	1104	−0.97
					10–11	3.1–5.1	590	−2174	2764	0.21
					24–25	4.0–6.5	675	−1932	2606	0.26

Deciduous Broadleaf & mixed conifers										
Hesse, France[4]	49°N, 7°E	300	924	335	30	6.0	238	–912	1150	0.21
Walker Branch, Tennessee, USA	36°N, 84°W	375	1261	249	60–90	6.0	470	–1038	1508	0.31
Park Fall, Wisconsin USA[5]	46°N, 90°W	485	1092	378	60–80	4.0	334	–817	1165	0.29
Harvard Forest, Massachusetts, USA[6]	43°N, 72°W	~335	970	416	90	5.5	280	–960	1210	0.23
							220	–930	1110	0.20
							140	–1140	1270	0.11
							210	–970	1170	0.18
							270	–810	1070	0.25
Willow Creek, Wisconsin, USA	46°N, 90°W	480	694	591	35–70	4.2	180	–769	949	0.19
Evergreen Broadleaf										
Castelporziano Italy[8]	42°N, 12°E	3	550	NA	1–2	0.7–2.0	–427	–2220	1420	–0.30
					50	3.5	381	–1160	1600	0.24
Tropical rainforest										
Manaus, Brazil[7]	3°S, 60°W	90	2080	957	mature	5.5	608	–2641	3249	0.19

[1]Law *et al.* (2002) carbon fluxes and water balances for 1996 or 1997.
[2]Paw *et al.* (2004) carbon fluxes for 1998–1999.
[3]Clark *et al*. (2004) carbon fluxes for 1996–1997 for recent clearcut and 10-year-old stand of slash pine; 1998–1999 for 24-year-old stand.
[4]Granier *et al.* (2000) carbon fluxes averaged for 1996 and 1997.
[5]Cook *et al.* (2004) carbon fluxes for 2000.
[6]Goulden *et al*. (1996) carbon fluxes for 1990 through 1994.
[7]Falge *et al*. (2002) carbon fluxes for 1995–1996; Malhi *et al*. (2002) water balance for 1995–1996.
[8]Kowalski *et al.* (2004) carbon fluxes, averaged for two years between 2000 and 2002.

fertility (Fig. 3.15) while that allocated to fine roots and mycorrhizae decreases proportionally (Hobbie, 2006).

Where model predictions deviate from direct measurement of NPP, the relative importance of climatic variation, soil fertility, and soil water storage can be assessed through sensitivity analyses (Rodriguez *et al.*, 2002). Such analyses indicate where additional field measurements might improve model predictions. Stand age is a variable that also must be recognized because older forests generally grow more slowly than younger ones on similar sites (Ryan *et al.*, 1997; Law *et al.*, 2004), but older forests may also have access to deeper soil resources through better developed root systems. Although young forests may exhibit high NPP, the correlation with NEP is contingent, as emphasized earlier, on recovery following disturbance (Fig. 10.3).

E. Trace Gas Emissions

A number of trace gases are produced directly as byproducts of photosynthesis or through the process of decomposition, as discussed in earlier chapters. Through field chamber measurements and continuous monitoring of trace gas emissions at eddy-flux tower sites, our understanding of the controls on trace gas emission has increased significantly in recent years.

In the tropics, the capacity of some tree species to produce isoprenes varies a hundredfold throughout the year (Kuhn *et al.*, 2004). The production of the carbon-based compounds is not related to LAI or canopy phenology but to seasonal changes in canopy photosynthetic activity (Fig. 10.4) and ambient air temperature (Chapter 6). It is reasonable that GPP should be more closely related to isoprene emissions in tropical forests than structural features such as LAI.

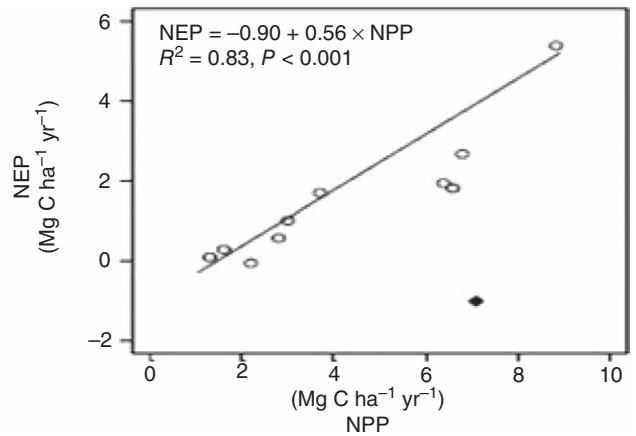

FIGURE 10.3. Net Ecosystem Production (NEP) increases linearly with Net Primary Production (NPP) except when forests are disturbed (black diamond). In the latter case, soil respiration is much enhanced. (After Pregitzer and Euskirchen, 2004.)

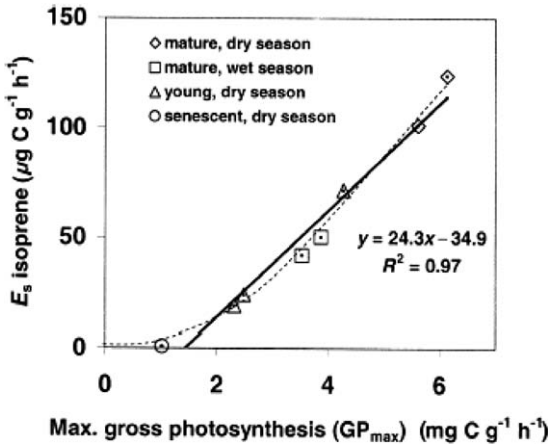

FIGURE 10.4. Seasonal variation in maximum GPP is closely correlated with isoprene production. (After Kuhn *et al*., 2004.)

To estimate emissions of NO_x, CO_2, and CH_4 from forested wetlands in both the boreal and subtropical region three models must be integrated: (1) a process-based forest growth model to calculate photosynthesis and its seasonal variation as a function of the environment; (2) a hydrologic model to predict water levels, O_2 concentrations, and water temperature; and (3) a biogeochemical model to compute the degree to which gas diffusion is limited by pore space and the availability of readily decomposable substrate in the soil (Cui *et al.*, 2005). With such integrated models the variation in solar radiation, soil water and oxygen levels, atmospheric N deposition, and substrate quality can be incorporated to predict seasonal differences in GPP, R_{a+h}, and CH_4 with considerable accuracy (Fig. 10.5).

F. Hydrologic and Energy Partitioning

By combining eddy-flux data from a wide range of evergreen and deciduous forests, as well as other types, Law *et al.* (2002) compared measurements of evapotranspiration (ET) when the canopy was dry against measurements of GPP at hourly, daily, weekly, and monthly time steps. Although considerable variation was observed hourly and daily, a linear correlation emerged when data were integrated and averaged at weekly or monthly intervals, showing how detailed analyses help identify appropriate periods for integration (Fig. 10.6).

Important hydrologic insight came from making measurements of volumetric water content, soil water potential, and root distribution at two drought-prone sites in the Pacific Northwest of the United States (Warren *et al.*, 2005). A comparison of diurnal and season changes in water content showed, with reference to eddy-flux measurements, that more than half the total water extracted by trees during the summer drought period came from a few roots that extended below a depth of 2 m. When the surface soil dries below water potentials experienced by nontranspiring trees (predawn values), water acquired by deep roots in zones of high potential is accessed. Some of this water is redistributed to surface

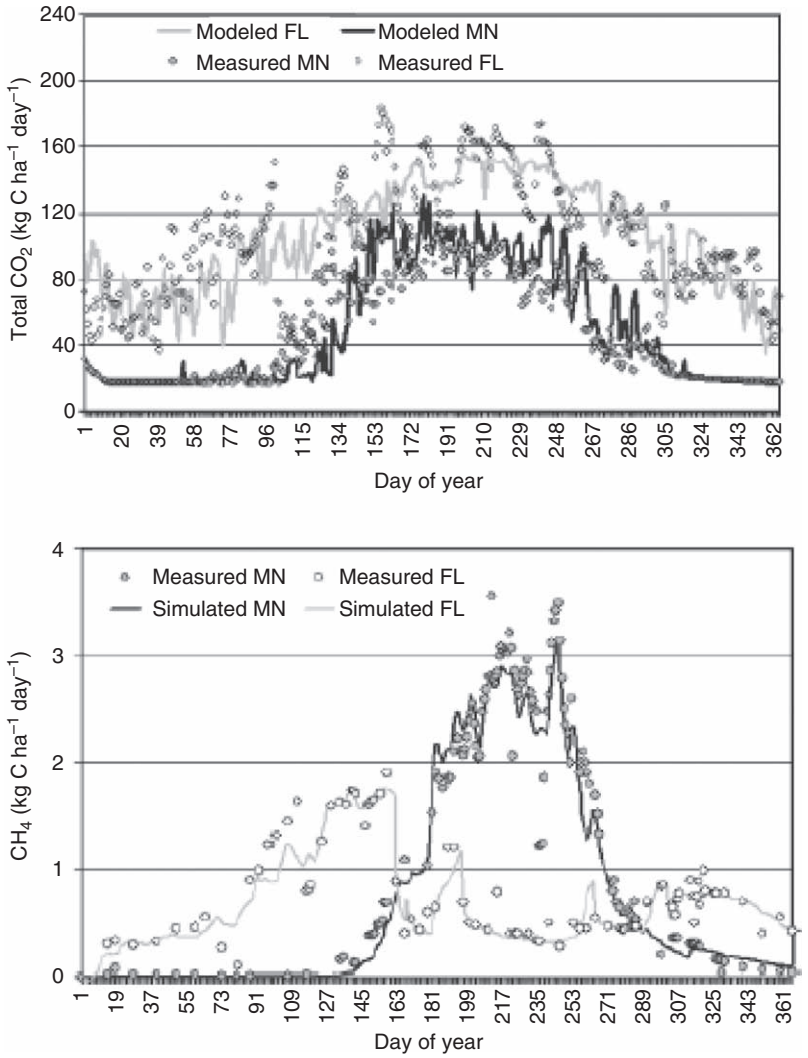

FIGURE 10.5. Through integration of three models, predictions of CO_2 and CH_4 efflux were compared for bogs in Minnesota (MN) and in Florida (FL). (After Cui *et al.,* 2005.)

roots and leaks out to the surrounding soil (Chapter 2; Fig. 2.15). Evidence of significant water transfer from deep to shallow soils during periods of drought makes it difficult to apply sophisticated soil-plant-atmosphere models that ignore this redistribution.

Alternatively, by monitoring seasonal variation in tree predawn water potential together with modeling (or measuring) daily water use via sap flux monitoring, a reasonable estimate of the total amount of available water in the rooting can be attained. With such knowledge it is not difficult to predict predawn tree water potential values and related seasonal changes in maximum canopy stomatal conductance (Fig. 2.13). Simplified models

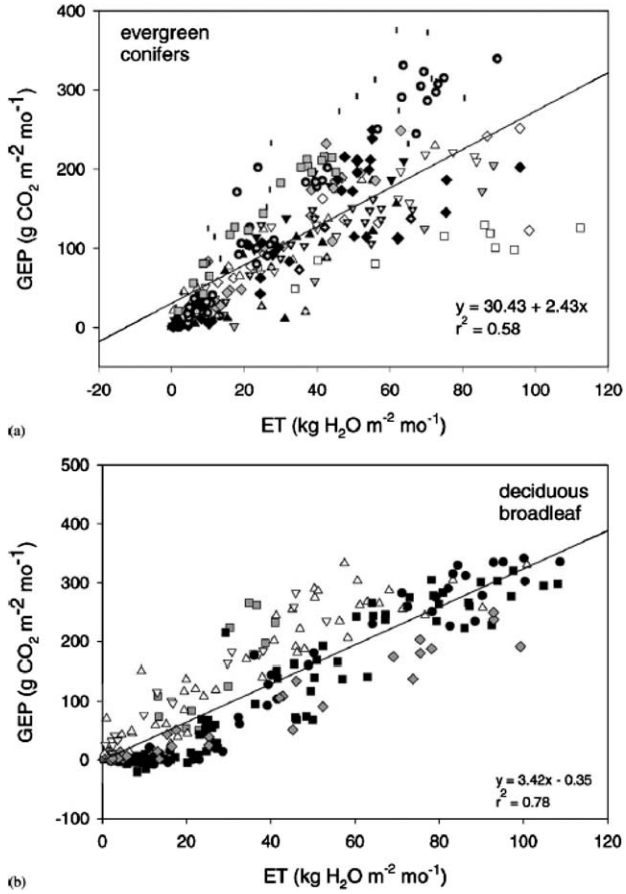

FIGURE 10.6. Where eddy-flux data were acquired at evergreen and deciduous forest sites over a number of years, a general relationship emerged between ET and gross ecosystem production (GEP) when comparisons were made at weekly (not shown) and monthly time steps. (After Law *et al*., 2002.)

such as Forest-BGC and 3-PG lend themselves readily to this approach (Coops *et al.*, 2001).

In Chapter 3 we recognized that diurnal and seasonal changes in ratio of sensible to latent heat losses (the Bowen ratio) offered a defining property of different types of vegetation that might be assessed by remote sensing and other means. The value of such Bowen ratio comparisons is demonstrated in Figure 10.7, based on energy balance analyses made at 20 eddy-flux tower sites throughout summer months.

G. Biogeochemistry

Although eddy-flux measurements now extend across a wide range of vegetation and environments, only one experiment to our knowledge has attempted to compare the impact of

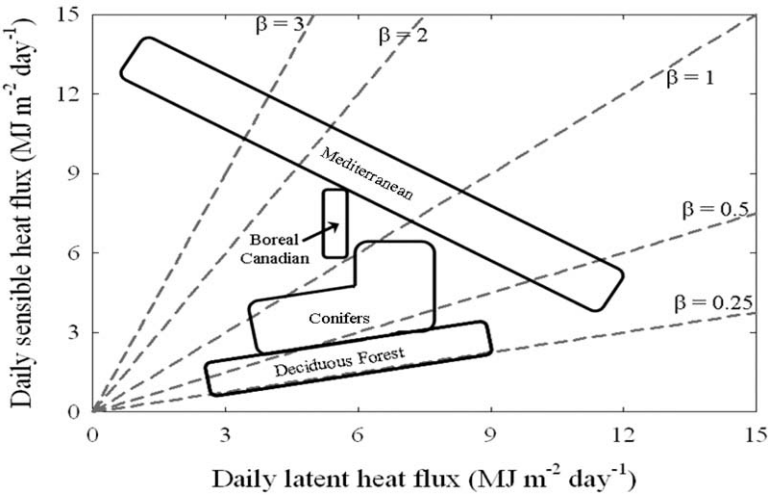

FIGURE 10.7. Distinct differences in the partitioning of energy between latent (vapor loss) and sensible heat (the Bowen ratio, β) allow separation of deciduous forests (n = 5), boreal coniferous forest (n = 5), temperate conifers (n = 6), and Mediterranean forests (n = 4). (After Wilson *et al.*, 2002.)

nitrogen deposition in the form of acid rain to forests. Beginning in 2001, 18 kg N ha^{-1} yr^{-1} were applied by helicopter to a spruce-hemlock forest in Maine. Initially, NEP measured at the treated area was ~5% lower than that measured at an untreated stand (Hollinger *et al.*, 2004). After three years of atmospheric N deposition net carbon uptake was ~8% higher at the fertilized than the untreated area.

Increased nitrogen loading interacts with the continued rise in atmospheric CO_2. This interaction has been documented at free-air carbon dioxide enrichment sites in North Carolina (Finzi *et al.*, 2002; Oren *et al.*, 2001). At canopy closure, CO_2 enrichment from ambient ~375 to 570 ppm increased NPP of *Pinus taeda* by only 14% on N deficient soils in contrast to 22% where supplements of N were added. These differences in growth responses may be the result of excess photosynthate acquired under elevated CO_2 being shifted to extract more nitrogen from the soil through the growth of fine roots and production of carbon-rich exudates. Sustained additions of nitrogen, through atmospheric deposition, commercial application of fertilizer, or through N-fixation can result in acidification of the soil and leaching of base cations (Chapter 6). In time, increased mortality may result, directly through nutrient imbalance, or indirectly by making trees more susceptible to insect and disease attack. This sequence of events appears to have occurred in unpolluted Douglas-fir forests of western Oregon as a result of conversion of stands of *Alnus*, a native nitrogen-fixing species, to extensive plantations of conifers that became infected with a needle cast disease when N/Ca ratios exceeded a critical threshold (Perakis *et al.,* 2006).

III. NEW REMOTE SENSING OF FORESTS

The latest generation of Earth-observing satellites provides significant improvements in radiometric sensitivity, geolocation accuracy, and spectral calibration over older sensors.

In addition, specific products are being generated for distribution in near-real time, thanks to the efforts of teams of scientists supported by sponsoring agencies such as NASA. The implications of these two advances are discussed in this section.

A. Canopy Fluxes

The accuracy of these new, more quantitative satellite data sets is being assessed in a variety of ways. For example, the global network of eddy-flux monitoring sites is being utilized to compare a range of variables predicted from satellite-derived information. There is a spatial analysis problem to scale from the approximately 1 km radius around a flux-tower that eddy covariance data represents (Schmid, 2002) to landscapes and large geographic areas. Figure 10.8 illustrates a conceptual framework to relate flux tower measurements to data acquired with satellites. For MODIS data, a project called "Bigfoot" developed a sampling protocol to estimate land cover and LAI around each flux tower (Cohen *et al.*, 2003). This project was repeated at many forested flux tower sites with promising results (Turner *et al.*, 2005). Some changes, however, were required in the initial algorithms to predict peak LAI estimates and land cover accurately (Cohen *et al*., 2003).

1. Gross Primary Production

Remote sensing allows us to expand predictions of GPP from individual stands to regions and continents. Since 2000, imagery from NASA's Moderate Resolution Imaging Spec-

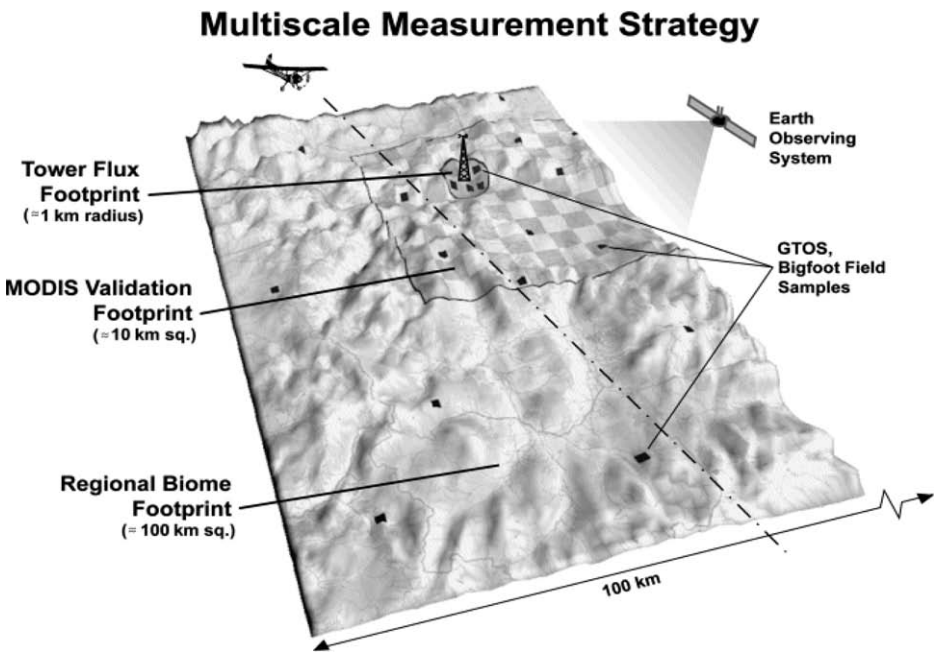

FIGURE 10.8. Integration of field and remote sensing measurements for landscape scaling of ecosystem fluxes. (After Running *et al*., 1999.)

troradiometer (MODIS), combined with extrapolations of coarse resolution weather data (1° latitude by 1.25° longitude), has yielded global scale estimates of GPP, averaged over eight-day intervals at 1 km resolution (Running *et al.*, 2004). The MODIS GPP product is calculated:

$$GPP = PAR \times FPAR \times \varepsilon_{max} (S_{Tmin} \times S_{vpd}) \quad (10.1)$$

where PAR represents incident photosynthetically active radiation, FPAR is the fraction of PAR absorbed by the plant canopy, ε_{max} is maximum quantum efficiency, and S_{Tmin} and S_{vpd} are, respectively, scalars for temperature minimum and vapor pressure deficits that are set to vary from 0 (shut down) to 1 (optimum).

The MODIS production efficiency model is simplified. It does not require information on soil water holding capacity, soil fertility, or daily precipitation. Where drought is important the assumption is made that sustained high vapor pressure deficits occur that suppress photosynthesis and ultimately reduce LAI and FPAR to a similar amount predicted by models that include a water balance. Rather than vary quantum efficiency as a function of soil fertility, ε_{max} is defined for representative types of vegetation within a biome.

Figure 10.9 illustrates how weekly flux tower measurements of GPP compare with MODIS satellite-derived estimates for a mature deciduous forest in upper Michigan, U.S.A., and for a Canadian boreal spruce forest. At both sites the seasonal patterns in GPP corresponded well, but MODIS satellite-derived values averaged 20 to 30% higher (Heinsch *et al.*, 2006). Such errors in MODIS-derived estimates of GPP reflect simplifications in the model that ignore reductions in photosynthesis as trees age and local variation in soil fertility, which affects ε_{max} (Zhao *et al.*, 2005). In addition, satellite-derived information on climatic conditions may not be representative when extrapolated (Zhao *et al.*, 2005). Where high quality meteorological data are available and canopy quantum effi-

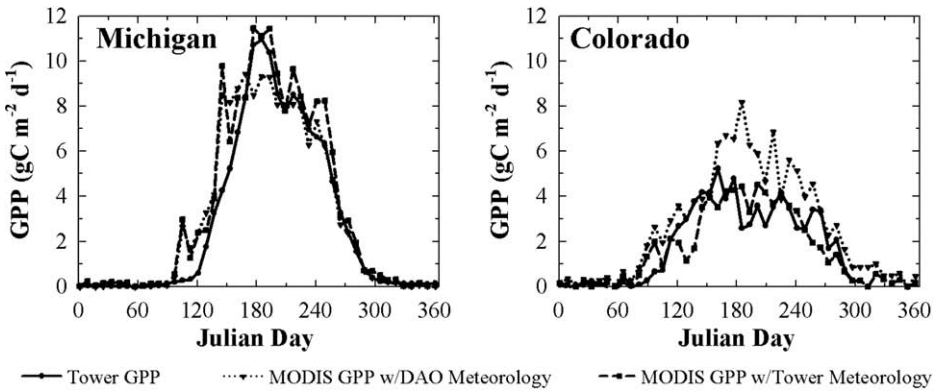

FIGURE 10.9. Comparison of daily gross primary production measured at an old growth deciduous broadleaf forest in Michigan and a subalpine fir forest in Colorado, U.S.A. with GPP derived from MODIS satellite data (Heinsch *et al*., 2006).

ciency is known, MODIS-derived estimates of GPP are close to those measured at tower sites (Turner *et al.,* 2006).

Another MODIS product, the enhanced vegetation index (EVI), provides improved estimates of FPAR and ε_{max} compared with the normalized difference vegetation index (NDVI) through addition of a blue spectral band in addition to near-infrared (NIR) and red (R) (Huete *et al.*, 2002). As a result, during the growing season, EVI has been linearly correlated with GPP measured at 10 widely dispersed eddy-flux tower sites (Rahman *et al.*, 2005).

2. Net Primary Production (NPP)

To predict variation in NPP across landscapes of increasing size requires progressive simplifications in models, as emphasized in Chapter 7 and discussed earlier. New global maps of MODIS-derived landcover, LAI, and annual NPP now are produced every year since 2000. Plates 14, 17, and 19 illustrate these new global datasets, which are available at http://edcimswww.cr.usgs.gov/pub/imswelcome/.

With increasing confidence in simplified formulations of stand growth models, their application has been expanded to estimate NPP across landscapes (Tickle *et al*., 2001) and regions (Whitehead *et al*., 2002; Swenson *et al*., 2005). As the spatial scale increases, model accuracy at any specific point tends to decrease, reflecting deficiencies in the reliability of climatic extrapolations, soil maps, and the ability to register details about the vegetation. Nonetheless, spatial patterns predicted in growth potential tend to follow those recorded in reference to scattered point measurements (Swenson *et al*., 2005).

Pan *et al.* (2006) used an innovative approach to map forest NPP for all of the northeastern United States (Fig. 10.10). A forest biogeochemistry model, PnET, was first run to identify local forest types, and to evaluate harvest impacts and soil water and nutrient

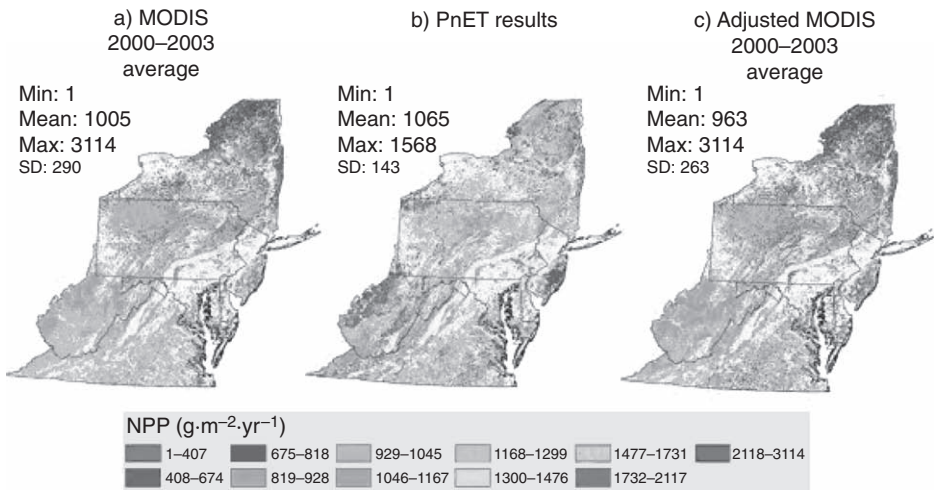

FIGURE 10.10. Calibration of MODIS satellite derived annual net primary production for the New England region with field inventory data to improve local accuracy (Pan *et al*., 2006). See Color Plate.

limitations on productivity. Global MODIS NPP products then were recalibrated to improve regional estimates, while retaining the comprehensive geographic coverage the satellite data provide.

Recently established forests are recognizable by their temporarily low leaf area indices. Once the canopy closes, differences exist between the greenness and wetness indices of reflected properties as forests age (Cohen *et al*., 2002). The standing biomass of forests is not a direct indicator of growth but a variable that new remote sensing tools in combination show increasing promise to estimate (Treuhaft *et al*., 2004; Lefsky *et al*., 2005a). If canopy height can be assessed at an accuracy of <1 m, periodic measurements at decadal intervals will provide a direct measure of growth (Lefsky *et al*., 2005b).

Throughout much of the world, forests are fairly young; thus estimates of leaf area index and related canopy properties are adequate measures from which to generate estimates of gross photosynthesis and autotrophic respiration, the latter a function of surface air temperature (Rahman *et al*., 2005). As a result, satellite-derived products of GPP and R_a together yield reasonable seasonal estimates of NPP at 8×8 km resolution globally (Running *et al*., 2004; Rahman *et al*., 2005). As with GPP, the extent that NPP can be modeled accurately independent of information on soils, precipitation, and canopy quantum efficiency is not fully known but is a recognized concern (Zhao *et al*., 2005).

3. Evapotranspiration

Daily evapotranspiration from flux tower data also has allowed development of a MODIS-driven ET for continental applications. Cleugh *et al.* (2007) compared daily ET data from two flux towers in Australia to evaluate how well various equations calculated seasonal drought constraints on ET. They ultimately chose the Penman-Monteith equation (Chapter 2) and, using MODIS landcover to define aerodynamic resistance and LAI, scaled surface resistance to compute daily ET (Fig. 10.11). Mu *et al.* (2007) produced the first global dataset from 2000 to 2005 of terrestrial daily evapotranspiration with this procedure. Even diurnal cycles of ET can be estimated at landscape scales by incorporating surface reflectance and radiometric temperature data at 15 to 30 minute intervals from geostationary satellites (Norman *et al.*, 2003).

4. Phenology

Improved satellite-derived estimates of large-scale forest phenology are now becoming available. Delbart *et al.* (2005) compared three spectral indices from the SPOT-VGT satellite to define the growing seasons of *Larix* and *Populus* forests in Siberia from 1999 to 2002. A NDSI = Normalized Difference Snow Index $(0.45\mu - 1.67\mu)/(0.45\mu + 1.67\mu)$ identified the end of snowmelt, whereas the NDVI = Normalized Difference Vegetation Index $(0.83\mu - 0.65\mu)/(0.83\mu + 0.65\mu)$ and NDWI = Normalized Difference Water Index $(0.83\mu - 1.67\mu)/(0.83\mu + 1.67\mu)$ recorded changes in canopy development throughout the growing season. In another study, Fisher *et al.* (2006) merged Landsat data with field observations to construct landscape-level phenological maps of deciduous forests for U.S. southern New England.

In the boreal zone, the seasonal transition from frozen to thawed conditions is a hydroecological trigger clearly detectable in the return backscatter of radar wavelengths. Kimball

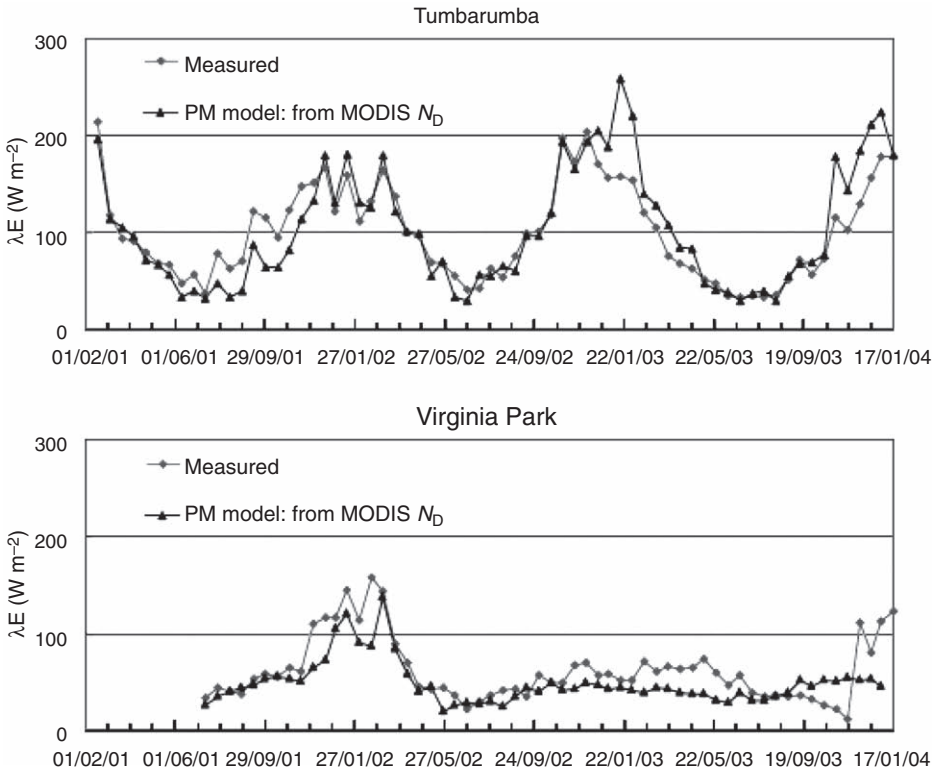

FIGURE 10.11. Comparison of daily evapotranspiration measured at a flux tower and derived from MODIS satellite data for a temperate (Tumbaramba) and savannah (Virginia Park) forests in Australia (Cleugh *et al*., 2007).

et al. (2004) employed an active radar sensor to record high-latitude seasonal freeze/thaw cycles and thus define the growing seasons for ten predominantly evergreen forests across western North America. While the radar sensor provides spatially coarse coverage (37 × 25 km), radar wavelengths penetrate clouds and offer temporal consistency unavailable from optical sensors (Fig. 10.12).

5. Canopy Chemistry

Canopy biochemical concentrations of Rubisco define the CO_2 uptake capacity of leaves, and are approximated by leaf N concentration. Green *et al*. (2003) found that 85% of the variation in ε_{max} in Equation 10.1 can be explained by leaf N concentration and specific leaf area. Hence, remote sensing of leaf N or chlorophyll would be valuable, but is not possible with broadband visible/IR sensors. New hyperspectral sensors typically have 200 to 300 spectral channels between 0.4 and 2.5 μ of high radiometric sensitivity, and currently are deployed from aircraft, providing much smaller 2 to 10 m, more homogeneous pixels than satellite sensors (Fig. 10.13). Zarco-Tejada *et al.* (2004) used narrow channels at 710 and 750 nm to estimate needle chlorophyll in *Pinus banksiana* near Ontario, Canada.

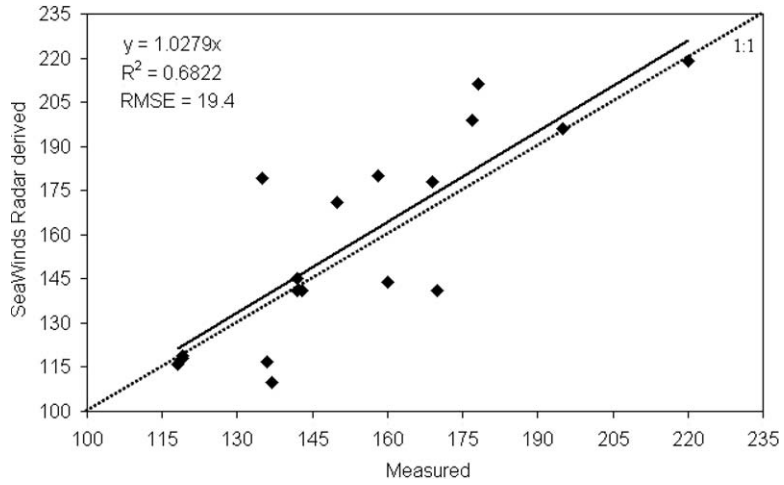

FIGURE 10.12. Estimates of growing season length in days yr^{-1} from SeaWinds radar data compared to measurements made at 10 boreal evergreen forest sites in North America. Radar wavelengths are particularly sensitive to freeze/thaw changes of the land surface (Kimball *et al*., 2004).

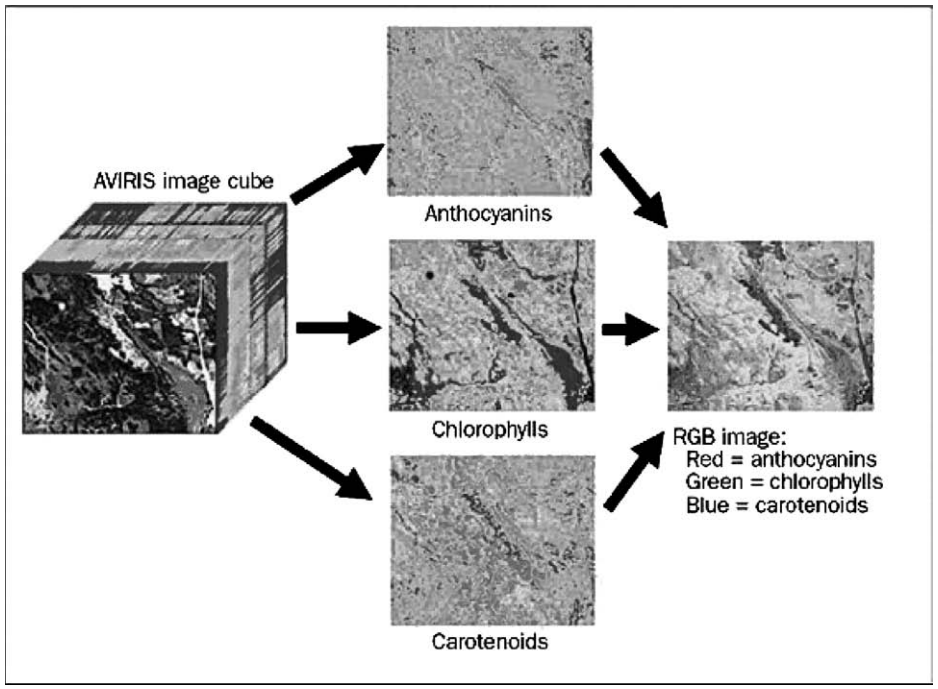

FIGURE 10.13. Classification of a Canadian boreal forest region based on relative leaf-pigment densities corresponding to different forest species derived from spectral mixture analysis of an Airborne Visible/Infrared Spectrometer dataset (Ustin *et al.*, 2004). See Color Plate.

Asner and Vitousek (2005) also demonstrated with hyperspectral data the possibility of distinguishing an overstory tree species from an N-fixing invading tree with two-fold differences in N-concentrations. Roberts *et al.* (2004) were able to identify six canopy species in the evergreen forests of western Washington based on a computed equivalent water thickness (EWT) using a selection of narrow spectral bands from AVIRIS.

Isolation of "red-edge," and SWIR reflectances from hyperspectral imagers has been shown to improve forest LAI estimation over broadband sensors such as MODIS (Lee *et al.*, 2004). However, hyperspectral data become difficult to interpret at landscape scales as multiple plant species and variations in illumination confound the signal.

B. Forest Structure

1. Lidar Measures of Structure and Biomass

Forest structure is important both for biogeochemical cycling, and to quantify other attributes such as wildlife habitat and fuel accumulations. Recent advances in lidar (light detection and ranging) show promise in being able to quantify canopy heights, stand density, and biomass. Airborne canopy lidar sensors fire a 1064 nm laser at over 1000 pulses per second at a canopy; the reflected signal is used to compute a vertical profile of structure (Fig. 10.14).

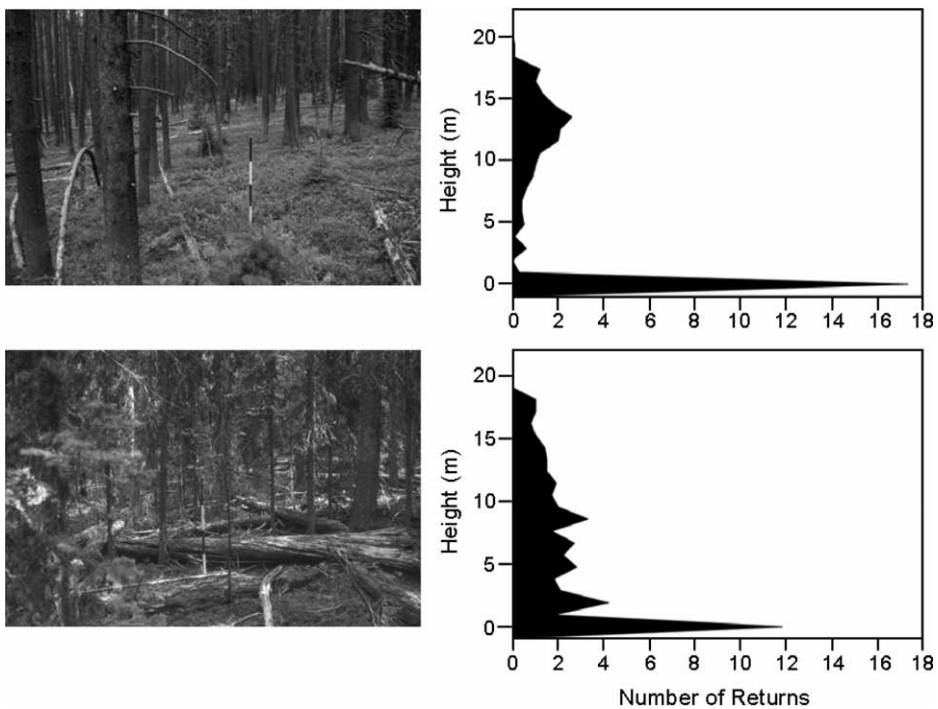

FIGURE 10.14. The vertical canopy profile of two *Pinus contorta* forests of differing density and structure in Montana measured by airborne scanning lidar (Seielstad *et al.*, 2005).

Lefsky *et al*. (2005a, 2005b) illustrated that airborne canopy lidar was able to estimate tree heights of forests in the Pacific Northwest ranging from 4 to 80 m and stand biomass from 10 to over 1000 Mg ha^{-1}. Airborne canopy lidars currently have only 2 km swath width, so profiling large areas is not yet feasible.

2. Forest Landcover and Disturbance

As we indicated in Chapter 9, launch of the EOS platforms and improved reprocessing of historical satellite datasets provide a new generation of global landcover datasets that contribute more realism to climate models and permit calculation of national carbon and hydrologic budgets (See and Fritz, 2006). The most valuable contribution of this new technology, however, may be the ability to quantify rates of disturbance and recovery. Lepers *et al.* (2005) report that beginning with the global satellite era from 1981, the Amazon represents the highest area of deforestation, and southeast Asia shows the largest areas of forest conversion to cropland. Forests in Siberia are recognized as being rapidly harvested whereas reforestation is occurring on areas that were previously in agricultural use in the southeastern United States and eastern China.

Major disturbances, primarily fire, have impacted an estimated 4 to 6 million $km^2\,yr^{-1}$, with highest frequencies in tropical savannahs (Potter *et al.*, 2002; Mouillot and Field, 2005). A global vegetation modeling analysis by Bond *et al.* (2005) suggests that humid tropical savannahs are sustained by fire, and quickly would revert to closed forest if fire were excluded. This suggests that climate change will impact forests more by increasing disturbance than by encouraging shifts in species distribution (Neilson *et al.*, 2005).

Figure 10.15 introduces an automated analysis of forest disturbance and recovery, using the ratio of *annual* maximum MODIS radiometric land surface temperature (LST) to the MODIS Enhanced Vegetation Index (EVI). Annual maximum LST increases and EVI decreases after a forest disturbance, resulting in an increase in DI value that returns to 1.0 as a forest grows in height and LAI recovers.

This DI quantified burnt areas in the western United Stated after the fire season of 2003 (Mildrexler *et al.*, 2007). As more years of global MODIS data are accumulated, our ability to distinguish natural variability from other causes will be further improved.

New hyperspatial (IKONOS at <1 m resolution) and airborne hyperspectral sensors such as AVIRIS with hundreds of spectral channels between 0.3 and 2.5 μ are now available to map local landcover change, although identification of individual species is not usually possible.

3. Forest Biodiversity

Sarr *et al*. (2005) provides a hierarchical framework for the analysis of species diversity at various geographic scales. Here we report on analyses at the regional level that complement previous studies reported at the global scale (Figs. 9.11 and 9.12). GPP, as explained earlier, is more accurately modeled than NPP. During the growing season, gross photosynthesis is the process shared in common among all tree species, deciduous and evergreen. NPP, on the other hand, differs significantly among species in the fraction allocated above- and belowground.

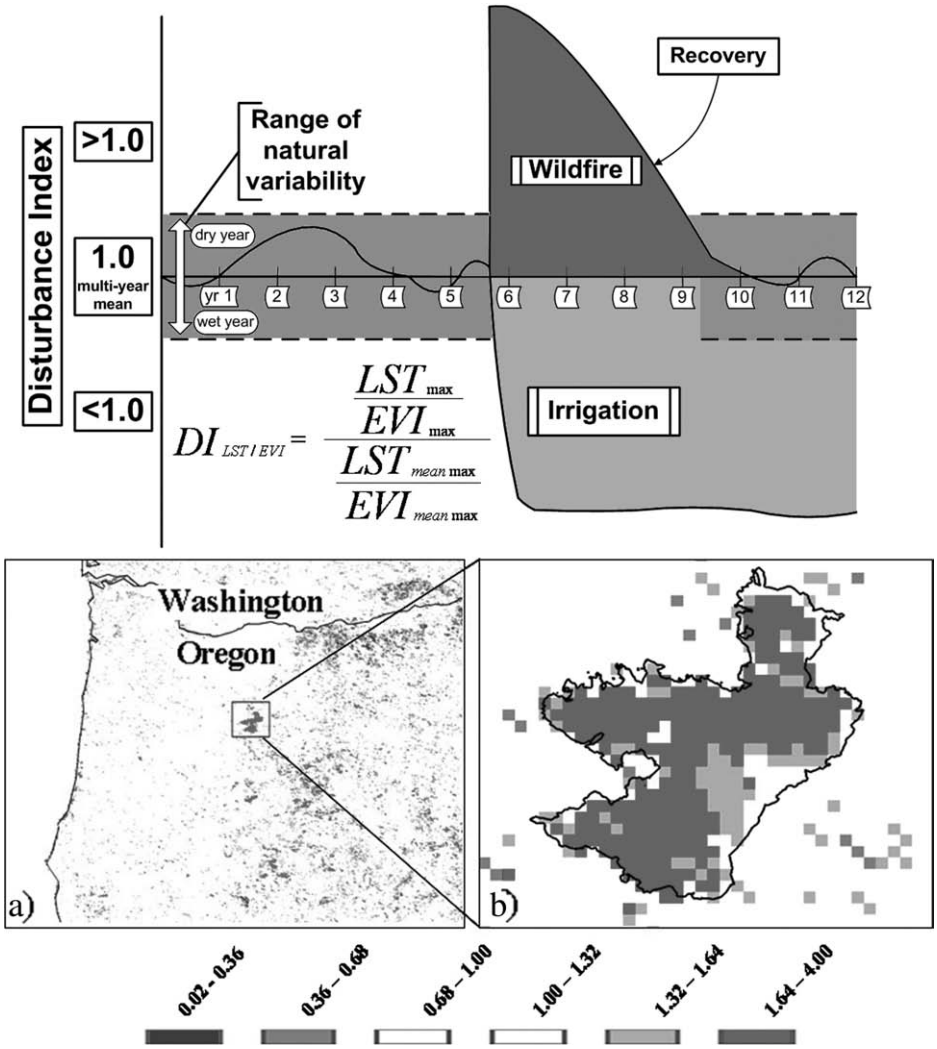

FIGURE 10.15. (a) A disturbance index (DI) uses annual maximum values of MODIS land surface temperature (LST) and Enhanced Vegetation Index (EVI) to detect yearly changes in forest cover and energy partitioning. (b) The DI detected the area burnt by a wildfire in Oregon closely matched that defined with more precise Landsat imagery (black line). (After Mildrexler *et al*., 2007). See Color Plate.

Across the U.S. Pacific Northwest, where GPP varies by more than 10-fold, Swenson and Waring (2006) report a polynomial (humped-shaped) relation between growing season GPP generated with 3-PG and tree species richness recorded on an equal number of survey plots within 100 km^2 units. This polynomial relation between GPP and tree richness emerged only when the full range in GPP was sampled. If the range in GPP is restricted, a positive, neutral, or even negative relationship results. The general explanation given for the observed pattern is that highly productive sites in the Pacific Northwest region contain a few fast-growing species that quickly develop a dense canopy that restricts the number of species present. Sites of intermediate productivity are unable to develop such dense canopies, and thus provide a haven for a wider range of species native to the region. On the harsher sites, the canopy is always sparse but few species are adapted to extreme drought, cold, and mechanical stresses that characterize such environments (Waring *et al*., 2002).

4. Wildlife Habitat

Hansen *et al.* (2002), using satellite data to interpret the productivity of forest land cover, evaluated bird species richness and habitat suitability (Fig. 10.16). Habitat suitability for birds was determined by combining a number of layers of information on topography and bioclimatology along with satellite-derived estimates of vegetation cover.

Both biodiversity and wildlife habitat analyses will ultimately benefit from the new lidar and radar technologies for measuring forest structure once data are available for large areas. Unmanned aerial vehicles (UAVs) may soon provide a more cost effective and controllable observation platform than orbiting satellites for regional analysis.

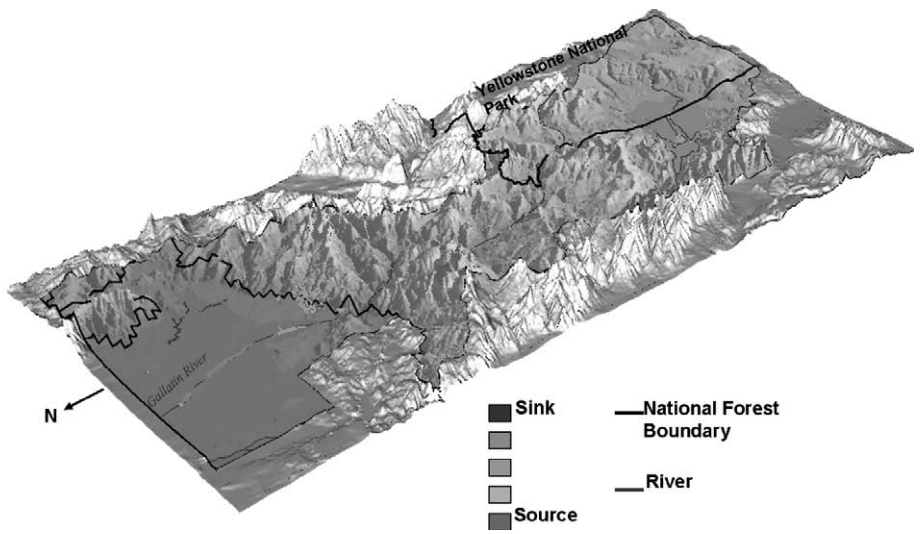

FIGURE 10.16. Richness in bird species vary across the greater Yellowstone area. Areas with high bird species richness are depicted in red. Green and tan colors indicate habitats with progressively fewer bird species. The areas with highest richness for the most part lay outside the National Park boundaries on private lands with higher productivity (Hansen *et al*., 2002). See Color Plate.

IV. CLIMATE CHANGE AND FORESTS

A. Climatic Trends

The average global air temperature has increased by 0.8°C ± 0.2°C over the last century, with the period since 1970 showing an acceleration to around 0.35°C/decade for the northern hemisphere and 0.16°C/decade for the southern hemisphere (IPCC AR4). Warming trends are highest in the northern boreal latitudes, 1–2°C, since 1970. Most of the warming has occurred in spring and winter, and minimum daily temperatures have increased more rapidly than maximums (Easterling *et al*., 1997; Boisvenue and Running, 2006; Bonsal *et al*., 2001).

Global precipitation trends are less consistent but overall show an increase of 3 to 5% in the last century (Groisman *et al*., 2004; Boisvenue and Running, 2006). This increase in precipitation does not necessarily mean more water available to forests. Higher air temperatures produce more evaporative water loss, and an increased fraction of annual precipitation falls as rain that immediately runs off rather than accumulates in snowpack (Knowles *et al*., 2006). Snowpack has decreased significantly over the last 30 to 50 years in the western United States as well as in Canada, and spring runoff is occurring one to four weeks earlier (Stewart *et al.*, 2005). Also, there is increasing evidence that wet climates are getting wetter and dry climates drier, with a resulting intensification of extremes in the hydrologic cycle. For example, streamflow has decreased in the western United States by about 20% over the last century (Rood *et al*., 2005), while in the eastern United States it has increased by 25% over the last 60 years (Groisman *et al*., 2004).

B. Impacts on Forests

Forests are responding to the previously mentioned climatic trends in numerous ways, the more obvious being through a change in phenology, tree growth rates, and the frequency and extent of disturbance. We summarize recent findings on these topics in this section.

1. Phenology

A comprehensive review of papers on global trends in phenology documents that growing seasons have lengthened by 10 to 20 days over the last 30 to 50 years (Linderholm, 2006). A phenology model developed from extensive field observations of lilac (*Syringa vulgaris*) in reference to meteorological records for the northern hemisphere indicate that the growing season increased by 1.7 days/decade from 1955 to 2000 (Fig. 10.17) (Schwartz *et al.*, 2006). A different analysis using global daily satellite data confirms that the onset of spring "greenness" is 10 to 14 days earlier than it was two decades ago across temperate latitudes in the northern hemisphere (Zhou *et al.*, 2001; Lucht *et al.*, 2002). Flowering dates of honeysuckle (*Lonicera japonica*) in the western United States have advanced by 3.8 days per decade (Cayan, 2001). The first leaves on aspen (*Populus tremuloides*) trees in Edmonton, Canada appear on average 26 days earlier than in 1901 (Beaubien and Freeland, 2000). This extension of the growing season should accelerate growth in temperature-limited forests where water is adequate.

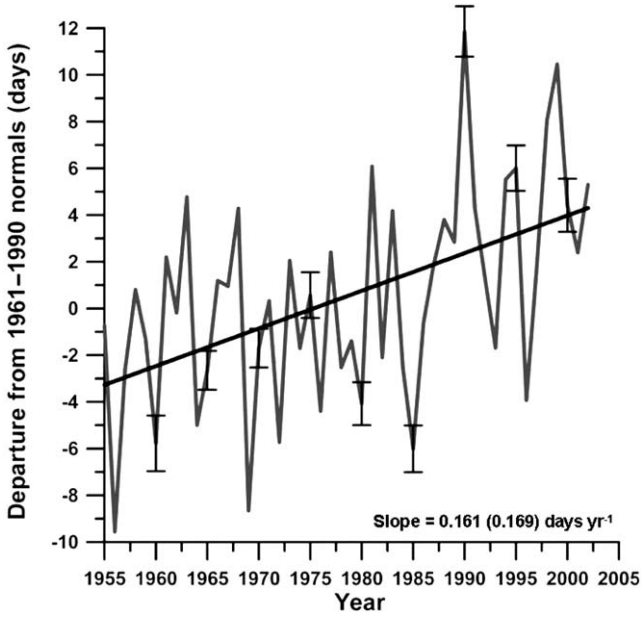

FIGURE 10.17. A lengthening growing season of the Northern Hemisphere is observed over the last 40 years. Calculations were based on daily temperature data and phenological observations following procedures described in Schwartz *et al.* (2006).

2. Forest Growth

Globally, total terrestrial net primary production on average has increased 6% between 1982 and 1999 based on satellite-derived assessments (Nemani, 2003; Cao *et al.*, 2002). However, this satellite-derived information, coupled with regional atmospheric CO_2 data acquired between 1982 and 2002, indicate a counterbalance between enhancement of photosynthetic activity in the spring and a depression of activity with increased summer drought in forests of the northern hemisphere (Angert *et al.*, 2005).

Field observations of forest growth support similar interpretation. A literature review of climatic influences on forest growth trends of the last 50 years found 37 of the 49 papers cited showed acceleration of forest growth (Boisvenue and Running, 2006). In North America, tree diameter growth has increased by about 1% per decade over the last century in areas with unfavorably low growing season temperatures (McKenzie et al., 2001; Joos, 2002; Caspersen, 2000). In the maritime part of eastern Canada, black spruce (*Picea mariana*) at the forest-tundra transition exhibit accelerated height growth since 1970 (Gamache, 2004). In Alaska, however, warming has adversely affected the water balance on south-facing slopes, causing white spruce (*Picea glauca*) to show reduced growth rates over the last 90 years (Barber et al., 2000).

Drought-prone forests in the southwestern United States also show decreasing growth since 1895, correlated with increasing evaporative demand attributed to rising air temperatures (McKenzie et al., 2001). Over the last century, tree growth at high elevations in the

Pacific Northwest has increased as the depth of the snowpack has dropped. At the same time, tree growth at lower elevations has been reduced, suggesting water limitations associated with increasing evaporative demand (Peterson and Peterson, 2001; Peterson *et al*., 2002).

For Europe as a whole, forest growth trends are generally positive. Vetter *et al.* (2005) attributed the increase in productivity of high elevation temperate conifer forests of Central Europe to an increase in N deposition between 1982 and 2001 and a similar response by conifer forests at mid- to low-elevations to the continued increase in atmospheric CO_2. The Swedish National Forest Inventory showed a highly significant annual increase in both height and basal area growth (0.5–0.8%) for the period 1953 to 1992 (Elfving *et al*. 1996) and site indices (SI), a measure of height attained at comparable ages, have increased for both Scots pine and Norway spruce during the last decades by 0.05 to 0.11 m/year (Ericksson and Karlsson, 1996). Site index of beech forests in Denmark also have shown an increase between 1920 and 1990 of 3.6 m (Skovsgaard and Henriksen, 1996).

Dendrochronological studies in France record an increasing growth trend over the past 150 years of 50% to 160% (Badeau *et al*., 1996). Forests in Switzerland also showed an improved growth trend from 4 to 49% since the beginning of the twentieth century (Bräker, 1996). In Austria, studies of Norway spruce show current annual increments have increased 17% since 1961 (Hasenauer *et al*., 1999; Schadauer, 1996). Beech forest in Slovenia increased current annual growth from 3.1 m^3/ha in 1947 to 5.3 m^3/ha in 1990 (Kotar, 1996). Analyses of carbon sequestration trends showed higher than expected rates of accumulation in 110-year old beech forests in Europe (Bascietto *et al*., 2004). On the other hand, growth analysis in Portugal indicates that Maritime pine, eucalyptus, and poplar made no measurable responses between 1970 and 1990, primarily because of water limitations (Tomé *et al*., 1996).

Across South America, an analysis of 50 long-term monitoring plots spanning years from 1971 to 2002 confirmed increases in stand basal area of 0.1 ± 0.04 m^2/ha/year (Lewis *et al*., 2004). All of these responses are not related to more intensive management or the use of commercial fertilizers. Forests appear to be responding to CO^2 fertilization, N-deposition, and longer growing seasons.

3. Net Forest Carbon Balances

Estimates of net ecosystem exchange, which represents the carbon balance of the land, can be derived from atmospheric inversion, carbon bookkeeping, and biogeochemical process models, augmented with satellite, field inventory, and flux tower data (House *et al*., 2003). Goodale *et al*. (2002) estimated a forest-sector carbon sink of 0.28 Pg C yr^{-1} for the contiguous United States. Canada, however, because of its generally lower rates of forest growth and increasing wildfires represented a source of 0.04 Pg C yr^{-1}. In Europe, the terrestrial carbon sink during the 1990s was estimated at 0.1 to 0.2 Pg C yr^{-1} (Janssens *et al*., 2001); forests are the major contributor to this sink (Janssens *et al*., 2004). These C-sequestration rates have increased significantly since the 1950s when the values were near 0.03 Pg C yr^{-1}. Since the 1990s, they have increased to 0.14 Pg C yr^{-1} based on extensive inventories of European forests. The strong carbon sink in European forests is attributed to an increase in growing season length and N-deposition (Fig. 10.18) (De Vries *et al.*, 2006).

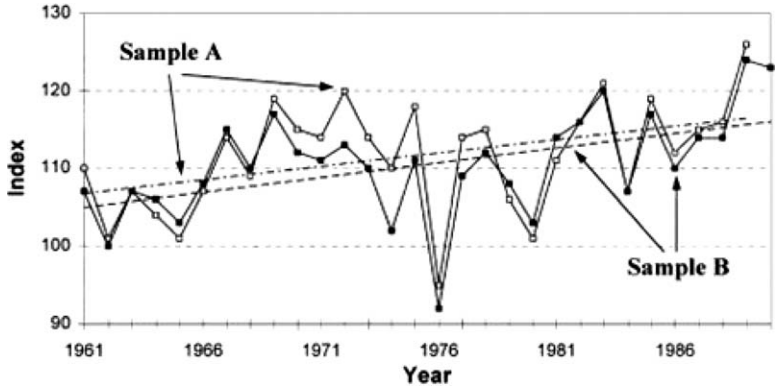

FIGURE 10.18. Mean annual increment growth of *Picea abies* in Austria measured on 614 (Sample A) and 565 (Sample B) growth plots increased on average by 10% between 1961 and 1990. An increase in average annual air temperature of 0.72°C best accounts for a lengthening of the growing season by 11 days over this period (Hasenauer *et al*., 1999).

4. Forest Disturbances

Climate change is altering the frequency, intensity, and duration of three major types of forest disturbances: wildfire, epidemics of pathogens, and windstorms (Dale *et al.*, 2001).

In recent decades, the area of forest burned has increased substantially. From 1920 to 1980, wildfires in the United States covered about 13,000 km^2/yr. Since 1980, the area has almost doubled to 22,000 km^2/yr, and for three of those years fires consumed 30,000 km^2 (Schoennagel *et al.*, 2004). The forested area burned between 1987 and 2003 is 6.7 times the area burned from 1970 to 1986, with a larger fraction of fires at higher elevations (Westerling *et al.*, 2006). In Canada, the area burned since 1990 averaged 30,000 km^2/yr, with three extreme years with between 60 and 76,000 km^2 consumed (Stocks *et al.*, 2002). Gillett *et al.* (2004) reported a correlation ($r = 0.77$) between warming summer temperatures of 0.8°C and the increase in the area burned by wildfires since 1970 in Canada.

A warming climate fosters wildfires by providing drier fuel and by creating meteorological conditions conducive to rapid spread (Westerling *et al.*, 2006). Earlier snowmelt, longer growing seasons, and higher summer temperatures combine to increase the frequency of wildfires (Fig. 10.19). In addition, in those parts of the world where fire suppression activities were most intensive, an uncharacteristically dense understory has developed along with an accumulation of dead woody material. These contribute, but do not override the effects of climatic change.

Insects and diseases are a natural part of all ecosystems. In forests, periodic insect epidemics kill millions of hectare of trees, providing heavy loads of potential tinder. The dynamics of these outbreaks are related to insect lifecycles that are tightly coupled to climate fluctuations (Williams and Liebhold, 2002). Many insects adapted to cold climates have a two-year lifecycle, so warmer winter temperatures increase larvae survival. As a result, spruce budworm in Alaska now completes its lifecycle in one year (Volney and

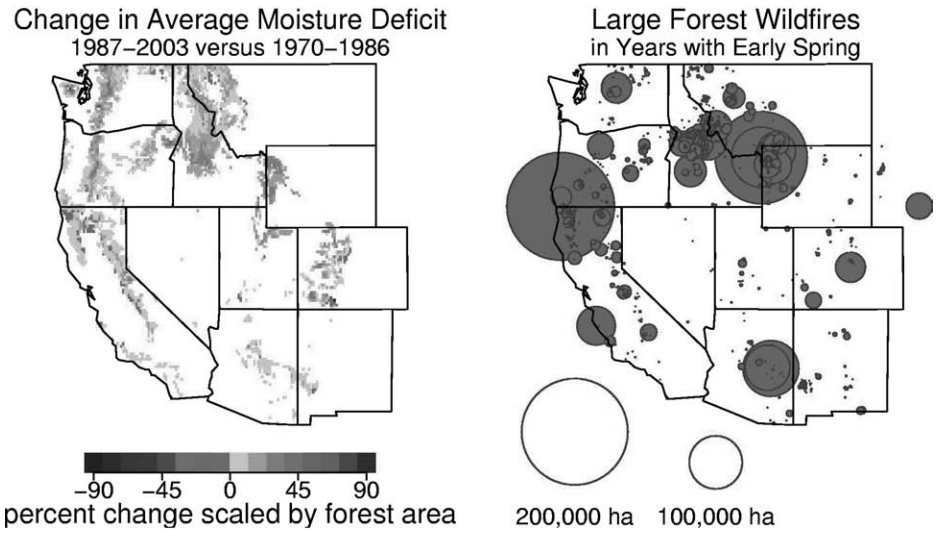

FIGURE 10.19. From 1970 to 2003, summertime moisture deficits increased dramatically in the western United States, and with a concurrent rise in wildfires >400 ha associated with an earlier melting of the snowpack in most years (Running, 2006; Westerling *et al*., 2006).

Fleming, 2000). Mountain pine beetles have expanded their range in British Columbia into areas previously too cold to support their survival (Carroll *et al.*, 2003). Multiyear droughts also reduce the available carbohydrates, limiting the ability of trees to generate defensive chemicals to repel insect attack (Logan *et al.*, 2003). Hogg *et al*. (2002) found recent dieback of aspen stands in Alberta to be caused by a combination of light snowpacks and drought in the 1980s that triggered defoliation by tent caterpillars, followed by damage from wood-boring insects and fungal pathogens.

Candau and Fleming (2005) studied the bioclimatic control of major spruce budworm defoliations in Ontario, Canada over an area of 400,000 km^2. Severe defoliations were associated with dry Junes when larvae are feeding, and mild winter temperatures that reduce winter mortality. Woods *et al*. (2005), however, attribute an unprecedented outbreak of *Dothisroma* needle blight on lodgepole pine in central British Columbia to increased summer precipitation. Even in mild temperate climates such as that of the southeast United States, higher winter and spring temperatures intensify southern pine beetle attacks (Gan, 2004). Although the relationships between changing climate and insect dynamics are complicated, there is a consensus that certain thresholds exist, that once exceeded, lead to dramatic increases in pests and pathogen outbreaks.

Although wind damage is common in forests worldwide, hurricanes (or typhoons as they are called in Asia) can in one event cause substantial disturbance over thousands of square kilometers. The hurricane season of 2005 damaged an estimated $5 billion worth of forests in the southeastern United States. McNulty (2002) estimates that a single large hurricane can reduce the annual carbon sequestration in all U.S. forests by 10%. New evidence suggests that climate change is increasing the power of hurricanes, which may

result in increasing windstorm-driven forest disturbance rates (Emmanuel, 2005; Webster *et al.*, 2005).

5. Changes in Forest Composition and Geographic Range

The most obvious shifts of forest biogeographical boundaries with current warming trends are shifts upward in the timberline and northward migration of boreal forests. In the southwestern United States, drought-adapted forests are migrating to higher elevations. In Colorado, photographs compared at timberline over a century show that aspen (*Populus tremuloides*) is replacing more cold-tolerant subalpine coniferous species (Elliott and Baker, 2004). Similarly, in the Yukon, lodgepole pine (*Pinus contorta*) is advancing into the zone previously dominated by the more cold-tolerant black spruce (Johnstone and Chapin, 2003). The subarctic treeline has risen at between 2 and 10 cm per year in northern Quebec over the last half-century (Gamache and Payette, 2005). These trends, predicted by nearly all ecosystem biogeography models, are expected to continue.

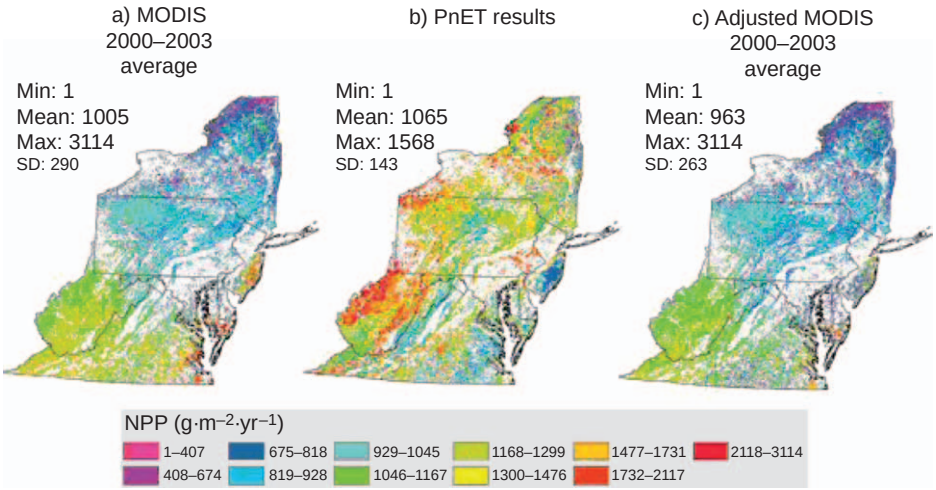

FIGURE 10.10. Calibration of MODIS satellite derived annual net primary production for the New England region with field inventory data to improve local accuracy (Pan *et al.*, 2006).

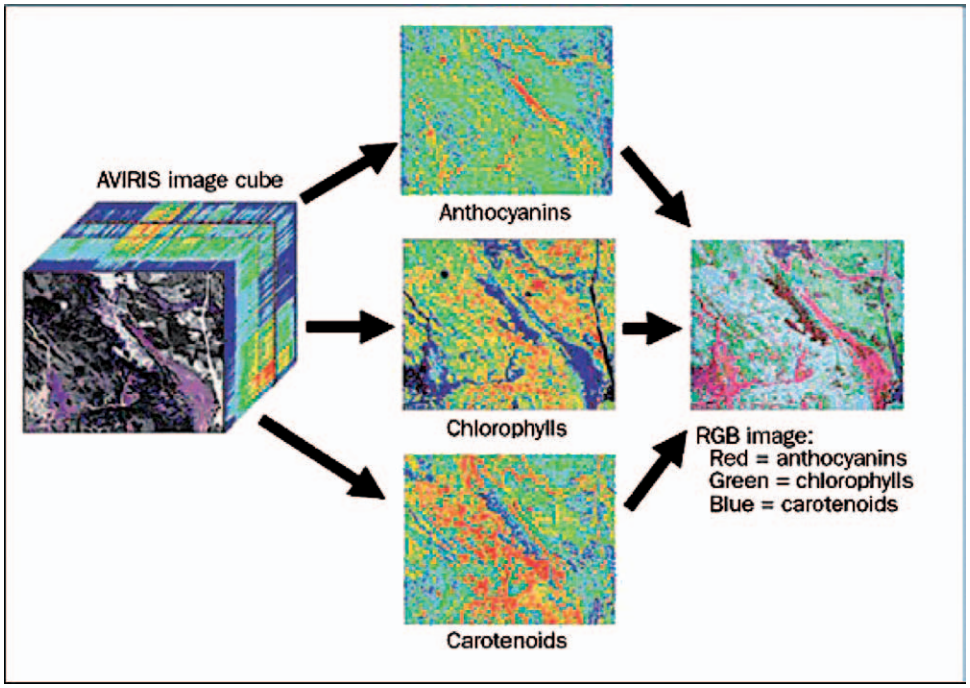

FIGURE 10.13. Classification of a Canadian boreal forest region based on relative leaf-pigment densities corresponding to different forest species derived from spectral mixture analysis of an Airborne Visible/Infrared Spectrometer dataset (Ustin *et al.*, 2004).

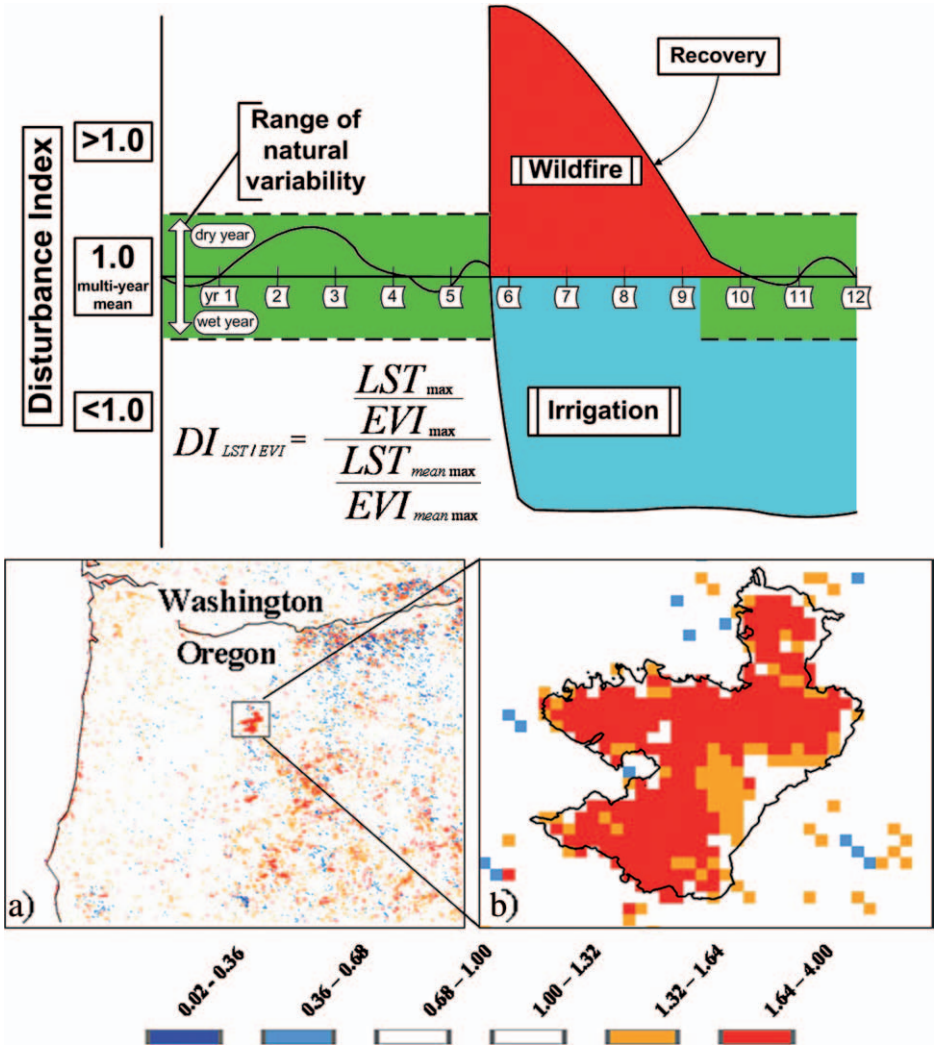

FIGURE 10.15. (a) A disturbance index (DI) uses annual maximum values of MODIS land surface temperature (LST) and Enhanced Vegetation Index (EVI) to detect yearly changes in forest cover and energy partitioning. (b) The DI detected the area burnt by a wildfire in Oregon closely matched that defined with more precise Landsat imagery (black line). (After Mildrexler *et al.*, 2007).

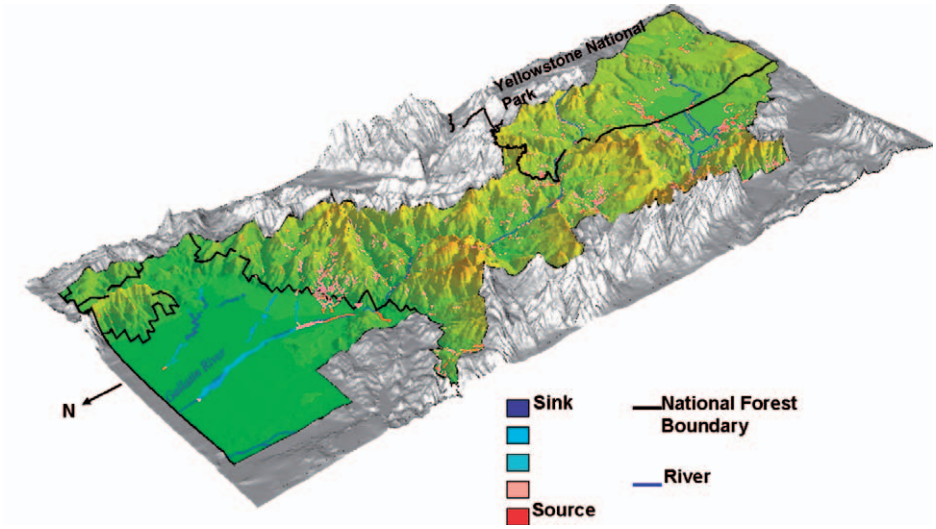

FIGURE 10.16. Richness in bird species vary across the greater Yellowstone area. Areas with high bird species richness are depicted in red. Green and tan colors indicate habitats with progressively fewer bird species. The areas with highest richness for the most part lay outside the National Park boundaries on private lands with higher productivity (Hansen *et al*., 2002).

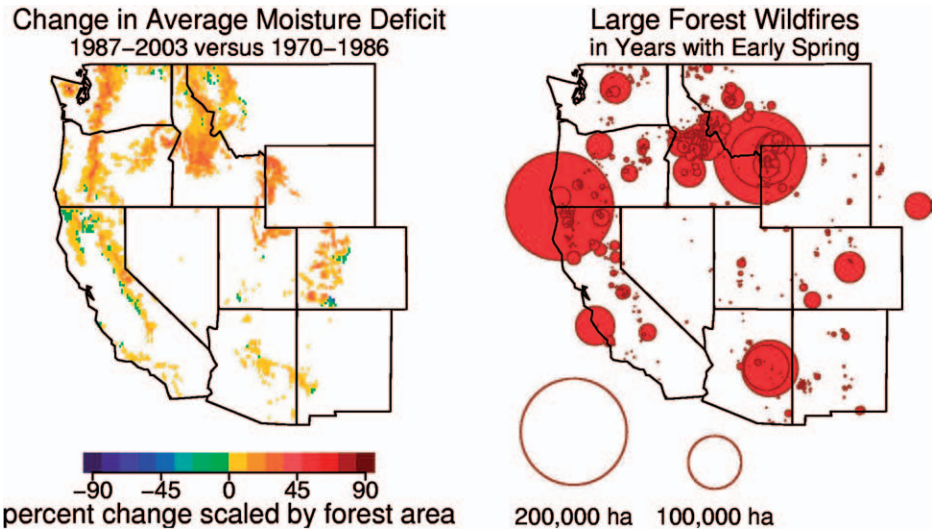

FIGURE 10.19. From 1970 to 2003, summertime moisture deficits increased dramatically in the western United States, and with a concurrent rise in wildfires >400 ha associated with an earlier melting of the snowpack in most years (Running, 2006; Westerling *et al*., 2006).